Toyoda H, Kumada T, Hayashi K, Honda T, Katano Y, Goto H, Kawaguchi T, Murakami Y, Matsuda F.	Antiviral combination therapy with peginterferon and ribavirin does not induce a therapeutically resistant mutation in the HCV core region regardless of genetic polymorphism near the IL28B gene.	***J Med Virol.***	83	1559-1564	2011
Terao C, Ohmura K, Katayama M, Takahashi M, Kokubo M, Diop G, Toda Y, Yamamoto N; Human Disease Genomics Working Group; Rheumatoid Arthritis (RA) Clinical and Genetic Study Consortium, Shinkura R, Shimizu M, Gut I, Heath S, Melchers I, Manabe T, Lathrop M, Mimori T, Yamada R, Matsuda F.	Myelin basic protein as a novel genetic risk factor in rheumatoid arthritis--a genome-wide study combined with immunological analyses.	***PLoS One***	6	e2045	2011
Onomoto K, Morimoto S, Kawaguchi T, Toyoda H, Tanaka M, Kuroda M, Uno K, Kumada T, Matsuda F, Shimotohno K, Fujita T, Murakami Y.	Dysregulation of IFN system can lead to poor response to pegylated interferon and ribavirin therapy in chronic hepatitis C.	***PLoS One.***	6	e19799	2011

Nakata I, Yamashiro K, Yamada R, Gotoh N, Nakanishi H, Hayashi H, Tsujikawa A, Otani A, Saito M, Iida T, Oishi A, Matsuo K, Tajima K, Matsuda F, Yoshimura N.	Association between the SERPING1 gene and age-related macular degeneration and polypoidal choroidal vasculopathy in Japanese.	***PLoS One***	6	e19108	2011
Terao C, Yamada R, Ohmura K, Takahashi M, Kawaguchi T, Kochi Y; Human Disease Genomics Working Group; RA Clinical and Genetic Study Consortium, Okada Y, Nakamura Y, Yamamoto K, Melchers I, Lathrop M, Mimori T, Matsuda F. The human	The human AIRE gene at chromosome 21q22 is a genetic determinant for the predisposition to rheumatoid arthritis in Japanese population.	***Hum Mol Genet.***	20	2680-2685	2011
Nakata I, Yamashiro K, Yamada R, Gotoh N, Nakanishi H, Hayashi H, Tsujikawa A, Otani A, Ooto S, Tamura H, Saito M, Saito K, Iida T, Oishi A, Kurimoto Y, Matsuda F, Yoshimura N.	Genetic variants in pigment epithelium-derived factor influence response of polypoidal choroidal vasculopathy to photodynamic therapy.	***Ophthalmology.***	118	1408-1415	2011

Hayashi H, Yamashiro K, Nakanishi H, Nakata I, Kurashige Y, Tsujikawa A, Moriyama M, Ohno-Matsui K, Mochizuki M, Ozaki M, Yamada R, Matsuda F, Yoshimura N.	Association of 15q14 and 15q25 with high myopia in Japanese.	***Invest Ophthalmol Vis Sci.***	52	4853-4858	2011
Murakami Y, Toyoda H, Tanaka M, Kuroda M, Harada Y, Matsuda F, Tajima A, Kosaka N, Ochiya T, Shimotohno K.	The progression of liver fibrosis is related with overexpression of the miR-199 and 200 families.	***PLoS One.***	6	e16081	2011
Li YJ, Goh L, Khor CC, Fan Q, Yu M, Han S, Sim X, Ong RT, Wong TY, Vithana EN, Yap E, Nakanishi H, Matsuda F, Ohno-Matsui K, Yoshimura N, Seielstad M, Tai ES, Young TL, Saw SM.	Genome-wide association studies reveal genetic variants in CTNND2 for high myopia in Singapore Chinese.	***Ophthalmology.***	118	368-375	2011

BJP British Journal of Pharmacology

DOI:10.1111/j.1476-5381.2012.01853.x
www.brjpharmacol.org

RESEARCH PAPER

Loss of multidrug and toxin extrusion 1 (MATE1) is associated with metformin-induced lactic acidosis

K Toyama[1], A Yonezawa[1], S Masuda[1], R Osawa[1], M Hosokawa[2], S Fujimoto[2], N Inagaki[2], K Inui[1,3] and T Katsura[1]

[1]*Department of Pharmacy, Kyoto University Hospital, Faculty of Medicine, Kyoto University, Kyoto, Japan,* [2]*Department of Diabetes and Clinical Nutrition, Graduate School of Medicine, Kyoto University, Kyoto, Japan, and* [3]*Kyoto Pharmaceutical University, Kyoto, Japan*

Correspondence
Toshiya Katsura, Department of Pharmacy, Kyoto University Hospital, Sakyo-ku, Kyoto 606-8507, Japan. E-mail: tkatsura@kuhp.kyoto-u.ac.jp

Keywords
H^+/organic cation antiporter; genetic variant; toxicodynamics; kidney; liver

Received
24 August 2011
Revised
5 December 2011
Accepted
5 January 2012

BACKGROUNDS AND PURPOSE

Lactic acidosis is a fatal adverse effect of metformin, but the risk factor remains unclear. Multidrug and toxin extrusion 1 (MATE1) is expressed in the luminal membrane of the kidney and liver. MATE1 was revealed to be responsible for the tubular and biliary secretion of metformin. Therefore, some *MATE* polymorphisms, that cause it to function abnormally, are hypothesized to induce lactic acidosis. The purpose of this study is to clarify the association between *MATE* dysfunction and metformin-induced lactic acidosis.

EXPERIMENTAL APPROACH

Blood lactate, pH and bicarbonate ion (HCO_3^-) levels were evaluated during continuous administration of 3 $mg \cdot mL^{-1}$ metformin in drinking water using *Mate1* knockout (–/–), heterozygous (+/–) and wild-type (+/+) mice. To determine the tissue accumulation of metformin, mice were given 400 $mg \cdot kg^{-1}$ metformin orally. Furthermore, blood lactate data were obtained from diabetic patients given metformin.

KEY RESULTS

Seven days after metformin administration in drinking water, significantly higher blood lactate, lower pH and HCO_3^- levels were observed in $Mate1^{-/-}$ mice, but not in $Mate1^{+/-}$ mice. The blood lactate levels were not affected in patients with the heterozygous *MATE* variant (*MATE1*-L125F, *MATE1*-G64D, *MATE2-K*-G211V). Sixty minutes after metformin administration (400 $mg \cdot kg^{-1}$, p.o.) the hepatic concentration of metformin was markedly higher in $Mate1^{-/-}$ mice than in $Mate1^{+/+}$ mice.

CONCLUSION AND IMPLICATIONS

MATE1 dysfunction caused a marked elevation in the metformin concentration in the liver and led to lactic acidosis, suggesting that the homozygous *MATE1* variant could be one of the risk factors for metformin-induced lactic acidosis.

Abbreviations

ALT, alanine aminotranferase; AST, aspartate aminotransferase; BUN, blood urea nitrogen; MATE, multidrug and toxin extrusion; MPP, 1-methyl-4-phenylpyridinium; OCT, organic cation transporter

Introduction

Metformin (*N,N*-dimethylbiguanide) is widely used in the treatment of type II diabetes mellitus. It exhibits pharmacological effects in the liver and is almost entirely excreted in urine in an unchanged form (Scheen, 1996). Lactic acidosis is a fatal adverse effect of biguanide agents including metformin (Bailey and Turner, 1996). It was reported that metformin-induced lactic acidosis was associated with an elevation in plasma concentrations of metformin in patients

© 2012 The Authors
British Journal of Pharmacology © 2012 The British Pharmacological Society

with renal failure (Pearlman *et al.*, 1996; Safadi *et al.*, 1996). However, it is noteworthy that metformin-induced lactic acidosis also occurs in patients without any risk factors (Tymms and Leatherdale, 1988; al-Jebawi *et al.*, 1998; Misbin *et al.*, 1998). These reports suggest that some risk factors in addition to renal impairment are associated with metformin-induced lactic acidosis.

Multidrug and toxin extrusion 1 (MATE1/SLC47A1) is expressed in the luminal membranes of renal proximal tubules and bile canalicular membranes of hepatocytes and is responsible for the efflux of cationic compounds, including metformin, from the cells (Otsuka *et al.*, 2005; Yonezawa and Inui, 2011). In the basolateral membranes of liver and kidney, organic cation transporters, OCT1 (SLC22A1) and OCT2 (SLC22A2), mediate metformin uptake from blood into cells respectively (Wang *et al.*, 2003; Kimura *et al.*, 2005). The renal clearance of metformin is five times higher than the glomerular filtration rate (Scheen, 1996), suggesting that the vectorial secretion via basolateral OCT2 and luminal MATE is important for the urinary excretion of metformin. Previously, we have demonstrated that the pharmacokinetics of metformin was significantly changed in *Mate1* knockout (*Mate1*$^{-/-}$) mice (Tsuda *et al.*, 2009). It was shown that the total body clearance and renal clearance was decreased to 25% and 18% in comparison with the wild-type (*Mate1*$^{+/+}$) mice, respectively. Therefore, it is thought that MATE1 determines the pharmacokinetics of metformin.

Transporter function is associated with inter-individual variations in drug responses. A *MATE1* rs2289669G>A variant located in the intron region was reported to be related to a glucose-lowering effect after metformin treatment in patients with diabetes, although little is known about the influence of the molecular mechanism of this variant on the MATE1 transporter (Becker *et al.*, 2009). In addition, it was reported that metformin elevates the blood lactate level in the presence of the MATE1 inhibitor pyrimethamine in mice, but under the conditions where the plasma concentration of metformin is much higher than those found in clinical situations (Ito *et al.*, 2010). These reports suggested that MATE1 function influenced the pharmacodynamics of metformin under these limited conditions. Previously, we and other groups have identified non-synonymous *MATE* variants with reduced or negligible transport activity (Chen *et al.*, 2009; Kajiwara *et al.*, 2009; Meyer zu Schwabedissen *et al.*, 2010). Taken together, these data indicate that functional impairment of MATE1 such as occurs with the genetic polymorphisms is involved in the lactic acidosis caused by metformin.

Here, we examined whether dysfunctional MATE1 caused metformin-induced lactic acidosis by using *Mate1* knockout mice as models of *MATE* variant carriers. In addition, we also investigated the effect of heterozygous *MATE* variants on blood lactate levels after metformin treatment both in mice and in humans. Our results indicated that MATE dysfunction is one of the risk factors for metformin-induced lactic acidosis.

Methods

Animals

Animals used in the present study were male C57BL/6 *Mate1*$^{+/+}$, *Mate1*$^{+/-}$ and *Mate1*$^{-/-}$ mice between 10 and 17 weeks of age. The methods used to generate the *Mate1* knockout mice were described previously (Tsuda *et al.*, 2009). In the present study, 6–12 mice were used in each experiment. Mice were kept in a temperature-controlled environment with a 14 h light and 10 h dark cycle, and received a standard diet and water *ad libitum*. All animal care and experimental procedures were conducted in accordance with *The Guidelines for Animal Experiments of Kyoto University*. All protocols were approved by the Animal Research Committee, Graduate School of Medicine, Kyoto University.

Long-term oral administration of metformin in mice

Mice (*Mate1*$^{+/+}$, n = 9; *Mate1*$^{+/-}$, n = 9; *Mate1*$^{-/-}$, n = 11) were given 3 mg·mL^{-1} metformin in drinking water for 21 days. One to four mice were kept in the same cage. The total volume of drinking water in each cage was measured at days 7, 14 and 21 to calculate the mean daily dosage of metformin. For blood collection, the mice were deprived of food (fasted) for 4 h before being anaesthetized with sodium pentobarbital (50 mg·kg^{-1} i.p.). Blood samples were collected from the tail vein, under 40 min of anaesthesia, before and at 7, 14 and 21 days after the administration of metformin. Blood lactate, pH and bicarbonate ion (HCO_3^-) levels were measured by an i-STAT analyser with a CG4+ cartridge (Fuso Pharmaceutical Industries, Osaka, Japan). Body weight was also measured at the same time. At the end of this experiment, blood samples were collected from the abdominal aorta, and aspartate aminotransferase (AST), alanine aminotranferease (ALT), blood urea nitrogen (BUN) and plasma creatinine levels were determined.

Single oral administration of metformin in mice

Mice were given 5 mL·kg^{-1} water (*Mate1*$^{+/+}$, n = 6; *Mate1*$^{-/-}$, n = 7) or 400 mg·kg^{-1} metformin (*Mate1*$^{+/+}$, n = 7; *Mate1*$^{-/-}$, n = 12) via oral gavage under 40 min of anaesthesia. To determine the baseline lactate level, blood samples were obtained by tail bleeding before the oral administration of metformin. At 24 h after oral administration, blood lactate levels and plasma concentrations of metformin were determined using blood samples obtained from the tail vein. Blood lactate levels were measured by Lactate Pro LT-1710 (Arkray Inc., Kyoto, Japan). At the end of this experiment, blood samples were collected from the abdominal aorta, and biochemical parameters were evaluated by i-STAT analyser with CG4+ and CHEM8+ cartridges (Fuso). Thereafter, mice were killed, and samples of the kidney, liver and skeletal muscle were obtained.

Metformin and lactate concentration–time profile in Mate1 knockout mice

Mate1$^{-/-}$ mice (n = 8) were deprived of food for 12 h before the administration of 150 mg·kg^{-1} metformin via oral gavage. Blood samples were obtained from the tail vein as before and at 0.5, 1, 2, 4 and 8 h after the oral administration metformin to measure blood lactate levels and plasma concentrations of metformin. Blood lactate levels were measured by Lactate Pro (Arkray).

Clinical study

Blood lactate and *MATE* genotype data were collected from patients, as described previously by Toyama *et al.* (2010). Of the 48 patients, lactate data were obtained from 29 patients receiving 250 mg of metformin in the morning. All were inpatients at the Department of Diabetes and Clinical Nutrition, Kyoto University Hospital. Patients were given metformin hydrochloride tablets (Melbin®, Dainippon Sumitomo Pharma Co. Ltd., Osaka, Japan) continuously for the treatment of diabetes mellitus. Blood lactate levels were measured at 0, 4 and 9 h after the administration of metformin using Lactate Pro (Arkray). This study was conducted in accordance with the Declaration of Helsinki and its amendments and was approved by Kyoto University Graduate School and the Faculty of Medicine, Ethics Committee.

Uptake experiments

The detail of the methods used for the metformin uptake experiments were as described previously (Tanihara *et al.*, 2007). Briefly, HEK293 cells (American Type Culture Collection CRL-1573, Manassas, VA, USA) were transfected with mouse Mate1, mouse Oct1, and mouse Oct2 cDNAs using Lipofectamine 2000 Reagent (Invitrogen, Carlsbad, CA, USA). The cells were incubated at 37°C for 1 or 2 min with incubation medium (pH = 7.4) containing [^{14}C]-metformin in the presence or absence of 5 mM 1-methyl-4-phenylpyridinium (MPP). Unlabelled metformin was added to [^{14}C]-metformin to obtain the final concentrations. The concentration-dependence of metformin transport by mouse Mate1, mouse Oct1 and mouse Oct2 was analysed by use of the Michaelis–Menten equation: $V = V_{max}[S] / (K_m + [S]) + K_d \cdot [S]$, where V is the transport rate, V_{max} is the maximal transport rate, [S] is the concentration of metformin, K_m is the Michaelis–Menten constant and K_d is a diffusion constant.

Analytical methods

Metformin concentrations in plasma, liver, kidney and skeletal muscle were determined by HPLC, as described previously (Kimura *et al.*, 2005). The methods used for sample pretreatment were as described in detail previously (Tsuda *et al.*, 2009). AST and ALT were measured by Transaminase C II-Test Wako (Wako Pure Chemical Industries Ltd., Osaka, Japan) according to the manufacturer's directions. Creatinine and BUN were measured by the LabAssay creatinine and UN *B*-test Wako (Wako Pure Chemical Industries Ltd.), respectively.

Materials

Metformin hydrochloride was obtained from Wako Pure Chemical Industries Ltd. [^{14}C]-metformin hydrochloride (54 mCi·mmol^{-1}) was purchased from Moravek Biochemicals, Inc. (Brea, CA, USA). MPP iodide was purchased from Sigma Aldrich (St. Louis, MO, USA). All other compounds used were of the highest purity available.

Statistical analysis

Data are expressed as the mean ± SEM. Data were analysed statistically using Student's unpaired *t*-test or one-way ANOVA with Dunnett's multiple comparison test. The data were analysed using GraphPad Prism 4.0 (GraphPad Software Inc., San Diego, CA, USA).

Results

Continuous oral administration of metformin in mice

Metformin-induced lactic acidosis was evaluated using *Mate1*$^{+/+}$, *Mate1*$^{+/-}$ and *Mate1*$^{-/-}$ mice. It was confirmed that the volume of drinking water without metformin was not different amongst the three genotypes. In the presence of metformin, the volume of drinking water was decreased in *Mate1*$^{-/-}$ mice, resulting in a reduction in the mean daily dose of metformin in *Mate1*$^{-/-}$ mice (7.0 mg·day^{-1}) compared with *Mate1*$^{+/+}$ (12.0 mg·day^{-1}) and *Mate1*$^{+/-}$ mice (11.4 mg·day^{-1}) (Figure 1A). Plasma concentrations of metformin were within the range for clinical use (*Mate1*$^{+/+}$, 1.4 ± 0.2; *Mate1*$^{+/-}$, 2.1 ± 0.3; *Mate1*$^{-/-}$, 4.2 ± 0.3 μg·mL^{-1}). There was no significant difference in body weight change amongst the three genotypes (Figure 1B). At 7, 14 and 21 days after metformin treatment, a higher blood lactate level was observed in *Mate1*$^{-/-}$ mice compared with those in *Mate1*$^{+/+}$ mice (Figure 1C). pH and HCO_3^- levels were significantly lower in *Mate1*$^{-/-}$ mice (Figure 1D and E). At day 21, there were no significant differences in AST, ALT and BUN between *Mate1*$^{+/+}$ and *Mate1*$^{-/-}$ mice (Table 1). In *Mate1*$^{+/-}$ mice, all parameters were comparable to those in *Mate1*$^{+/+}$ mice (Figure 1C–E).

Blood lactate levels in diabetic patients

Because of the limited number of patients examined (n = 48), no homozygous *MATE* variant carrier was found in this clinical study. Heterozygous *MATE* variants have little influence on the metformin plasma concentration and oral clearance as described previously (Toyama *et al.*, 2010). In the present study, the effect of metformin on blood lactate levels was examined in 29 patients receiving 250 mg of metformin. Four heterozygous *MATE*-variant carriers were found; one patient carried *MATE1*-L125F variant, two carried *MATE1*-G64D variant and one carried *MATE2-K*-G211V variant. As expected, there was no significant difference in blood lactate levels between the two groups (Figure 2).

Single oral administration of metformin in mice

Based on the present data, no functional difference in the *MATE1* heterozygous genotype in comparison with the wild-type was observed *in vivo*, and therefore, we focused on the difference between the *Mate1*$^{+/+}$ and *Mate1*$^{-/-}$ mice. In the long-term administration experiment, the pharmacokinetics of metformin in *Mate1*$^{+/+}$ and *Mate1*$^{-/-}$ mice could not be rigorously evaluated because of the different dosages between the two groups. Therefore, the blood lactate levels and the pharmacokinetics of metformin were investigated in *Mate1*$^{+/+}$ and *Mate1*$^{-/-}$ mice after a single oral dose. In the vehicle-treated mice, there was no significant difference between these parameters in *Mate1*$^{+/+}$ and *Mate1*$^{-/-}$ mice. In metformin-treated mice, two *Mate1*$^{-/-}$ mice died and blood lactate levels were significantly high in *Mate1*$^{-/-}$ mice compared with

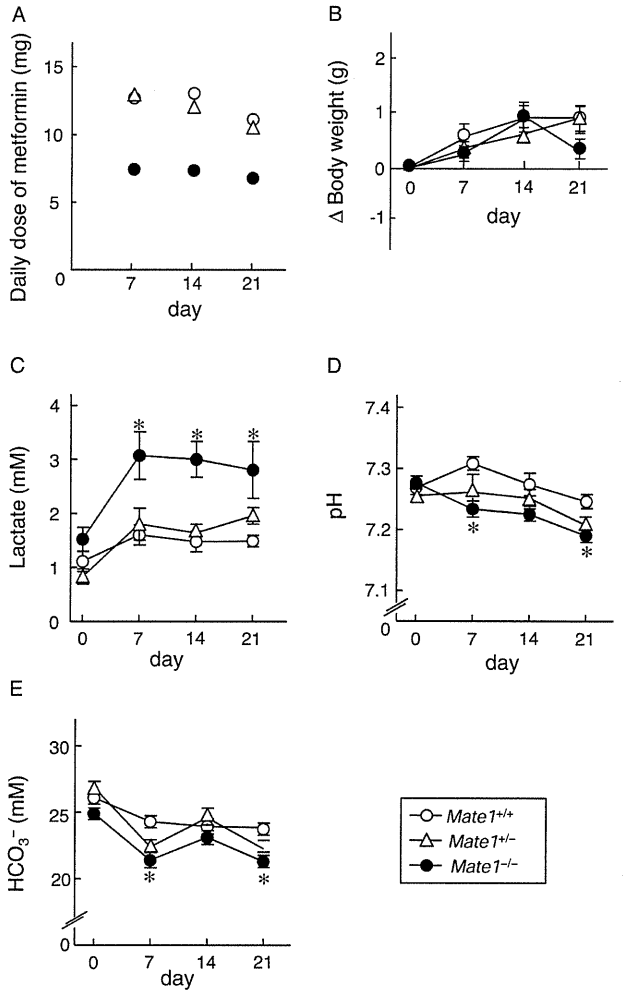

Figure 1

Long-term toxicity of metformin in *Mate1*$^{+/+}$, *Mate1*$^{+/-}$ and *Mate1*$^{-/-}$ mice. *Mate1*$^{+/+}$ (n = 9), *Mate1*$^{+/-}$ (n = 9) and *Mate1*$^{-/-}$ (n = 11) mice were given 3 mg·mL^{-1} metformin in drinking water for 21 days. The mean daily dose of each 7 days (A), body weight change from baseline (B), blood lactate level (C), pH (D) and HCO_3^- levels (E) were determined at 0, 7, 14 and 21 days after metformin treatment. Blood samples were collected under anaesthesia in 4 h-fasted mice. Blood lactate, pH and HCO_3^- levels were measured by i-STAT. Each point represents the mean ± SEM. *P < 0.05, significantly different from *Mate1*$^{+/+}$ mice at each day.

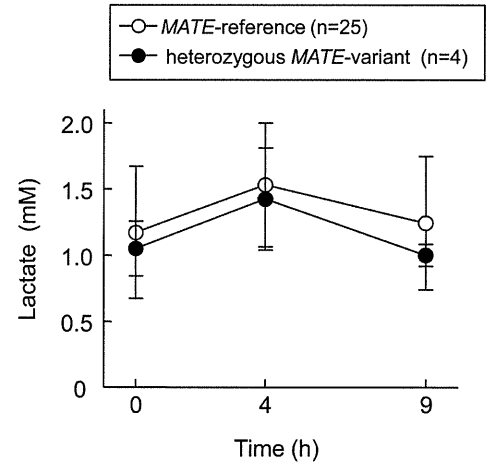

Figure 2

Lactate concentration–time profile in diabetic patients. Metformin was administered to patients in the *MATE*-reference group (n = 25) and heterozygous *MATE*-variant group (n = 4). Blood lactate levels were measured by Lactate Pro at 0, 4 and 9 h after the oral administration of metformin. One *MATE1*-L125F variant carrier, two *MATE1*-G64D variant carriers and one *MATE2-K*-G211V variant carriers were found in this study. Each point represents the mean ± SD.

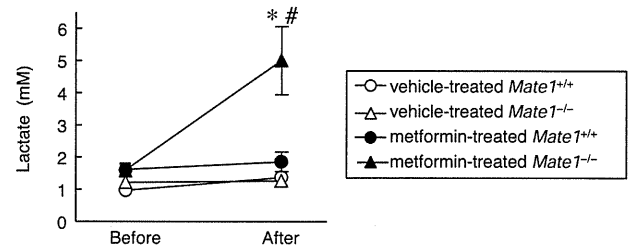

Figure 3

Blood lactate level in vehicle- or metformin-treated *Mate1*$^{+/+}$ and *Mate1*$^{-/-}$ mice after a single dose of metformin. All mice were given 400 mg·kg^{-1} metformin via oral gavage. Blood lactate levels were determined before and 24 h after the oral administration of metformin in vehicle-treated *Mate1*$^{+/+}$ mice (n = 6), vehicle-treated *Mate1*$^{-/-}$ mice (n = 7), metformin-treated *Mate1*$^{+/+}$ mice (n = 7) and metformin-treated *Mate1*$^{-/-}$ mice (n = 10). Each point represents the mean ± SEM. *P < 0.05, significantly different from vehicle-treated mice with the same genotype. $^{\#}P$ < 0.05, significantly different from metformin-treated *Mate1*$^{+/+}$ mice.

Mate1$^{+/+}$ mice (Figure 3). Several other biochemical parameters were also evaluated (Table 2). The pH and HCO_3^- levels were lower in metformin-treated *Mate1*$^{-/-}$ mice than in metformin-treated *Mate1*$^{+/+}$ mice. In addition, the base excess of extracellular fluid as an indicator of metabolic acidosis was also significantly decreased in metformin-treated *Mate1*$^{-/-}$ mice compared with metformin-treated *Mate1*$^{+/+}$ mice.

Plasma concentrations of metformin were 15-fold higher in *Mate1*$^{-/-}$ mice than in *Mate1*$^{+/+}$ mice (Figure 4A). Metformin concentrations in the kidney, liver and skeletal muscle were also 21-, 69- and 44-fold higher in *Mate1*$^{-/-}$ than those in *Mate1*$^{+/+}$ mice, respectively (Figure 4B, D and F). In *Mate1*$^{-/-}$ mice, the apparent tissue-to-plasma concentration ratio (K_p) was higher in the liver and skeletal muscle, but not in the kidney (Figure 4C, E and G).

Metformin and lactate concentration–time profile in mice

To clarify the association between the PK/PD profile, we examined the metformin and lactate concentration–time profile in *Mate1*$^{-/-}$ mice. The blood lactate level increased later than the plasma concentration of metformin; the plasma

Table 1

Biochemical parameters in *Mate1*$^{+/+}$, *Mate1*$^{+/-}$ and *Mate1*$^{-/-}$ mice 21 days after metformin treatment

	Mate1$^{+/+}$	*Mate1*$^{+/-}$	*Mate1*$^{-/-}$
Hepatic function			
AST (IU·L^{-1})	24 ± 3	21 ± 2	21 ± 2
ALT (IU·L^{-1})	33 ± 4	23 ± 1	20 ± 1
Renal function			
Creatinine (mg·mL^{-1})	0.0035 ± 0.0001	0.0038 ± 0.0001	0.0044 ± 0.0001*
BUN (mg·mL^{-1})	0.22 ± 0.02	0.23 ± 0.02	0.22 ± 0.01
Acid-base balance			
Lactate (mM)	1.5 ± 0.1	2.0 ± 0.2	2.8 ± 0.6*
pH	7.24 ± 0.01	7.21 ± 0.02	7.19 ± 0.01*
HCO_3^- (mM)	24 ± 1	22 ± 1	21 ± 0*

Mate1$^{+/+}$ (n = 9), *Mate1*$^{+/-}$ (n = 9) and *Mate1*$^{-/-}$ mice (n = 11) were used.
*P < 0.05, significantly different from *Mate1*$^{+/+}$ mice.

Table 2

Biochemical parameters and body weight in vehicle- or metformin-treated *Mate1*$^{+/+}$ and *Mate1*$^{-/-}$ mice.

	Vehicle		Metformin	
	Mate1$^{+/+}$	*Mate1*$^{-/-}$	*Mate1*$^{+/+}$	*Mate1*$^{-/-}$
BW (g)	30 ± 1	27 ± 1	29 ± 1	27 ± 0
pH	7.32 ± 0.02	7.28 ± 0.03	7.29 ± 0.02	7.03 ± 0.10**$^{\#\#}$
pCO_2 (mmHg)	50 ± 3	51 ± 4	48 ± 3	39 ± 3*
pO_2 (mmHg)	109 ± 17	114 ± 14	121 ± 4.1	127 ± 12
BE_{ecf} (mM)	−1 ± 1	−3 ± 1	−4 ± 1	−16 ± 2***$^{\#\#\#}$
HCO_3^- (mM)	25 ± 1	24 ± 1	23 ± 1	12 ± 2***$^{\#\#\#}$
TCO_2 (mM)	27 ± 1	25 ± 1	24 ± 1	15 ± 2***$^{\#\#\#}$
sO_2 (%)	96 ± 2	97 ± 1	98 ± 0	95 ± 1
Na (mM)	148 ± 1	151 ± 1	148 ± 1	153 ± 1$^{\#\#}$
K (mM)	5.5 ± 0.5	4.7 ± 0.2	4.9 ± 0.2	5.2 ± 0.2
Cl (mM)	116 ± 1	120 ± 1	117 ± 1	131 ± 0***$^{\#\#\#}$
iCa (mM)	1.3 ± 0.0	1.3 ± 0.0	1.3 ± 0.0	1.3 ± 0.1
Glu (mg·mL^{-1})	2.03 ± 0.16	1.78 ± 0.13	1.76 ± 0.09	1.44 ± 0.10*$^{\#}$
Hct (%PCV)	43 ± 2	42 ± 1	39 ± 1	42 ± 1
Hb (g·mL^{-1})	0.15 ± 0.01	0.14 ± 0.00	0.13 ± 0.00	0.14 ± 0.00
AnGap (mM)	15 ± 1	15 ± 0	15 ± 1	16 ± 1
BUN (mg·mL^{-1})	0.24 ± 0.04	0.24 ± 0.01	0.19 ± 0.05	0.45 ± 0.11
Creatinine (mg·mL^{-1})	0.0034 ± 0.0010	0.0036 ± 0.0002	0.0030 ± 0.0001	0.0054 ± 0.0008

Vehicle-treated mice (*Mate1*$^{+/+}$, n = 6; *Mate1*$^{-/-}$, n = 7), metformin-treated mice (*Mate1*$^{+/+}$, n = 7; *Mate1*$^{-/-}$, n = 10).
*P < 0.05, **P < 0.01, ***P < 0.001, significantly different from vehicle-treated mice with the same genotype; $^{\#}P$ < 0.05, $^{\#\#}P$ < 0.01, $^{\#\#\#}P$ < 0.001, significantly different from *Mate1*$^{+/+}$ mice.
BW, body weight; pCO_2, partial pressure of carbon dioxide; pO_2, partial pressure of oxygen; BE_{ecf}, base excess of extracellular fluid; TCO_2, total carbon dioxide; sO_2, saturation oxygen; iCa, ionized calcium; Glu, glucose; Hct, haematocrit; Hb, haemoglobin; AnGap, anion gap.

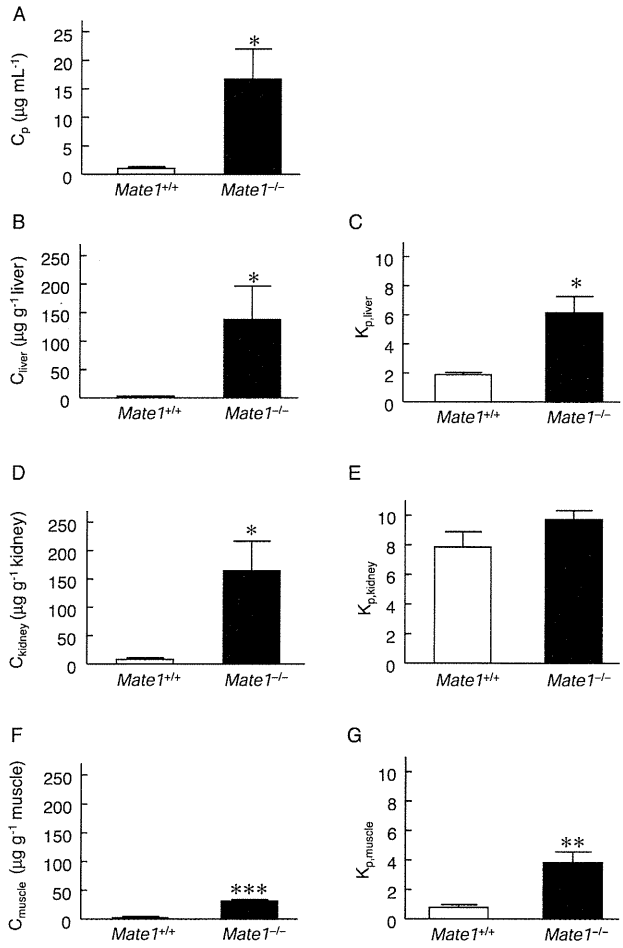

Figure 4

Pharmacokinetics of metformin in *Mate1*$^{+/+}$ and *Mate1*$^{-/-}$ mice after a single dose of metformin. In the same mice as shown in Figure 3, metformin concentrations in plasma (A), liver (B), kidney (D) and skeletal muscle (F) were determined by HPLC. K_p values in the liver (C), kidney (E) and skeletal muscle (G) were calculated by dividing the tissue concentration by the plasma concentration of metformin. Data represent mean ± SEM. *P < 0.05, **P < 0.01, ***P < 0.001, significantly different from *Mate1*$^{+/+}$ mice.

concentration of metformin and blood lactate level peaked at 2 and 4 h, respectively, after the oral administration metformin in these mice (Figure 5).

Concentration-dependence of [^{14}C]-metformin uptake by mouse Mate1, mouse Oct1 and mouse Oct2

We examined the characteristics of metformin transport by mouse Mate1, mouse Oct1 and mouse Oct2. The uptake of [^{14}C]-metformin by mouse Mate1, mouse Oct1 and mouse Oct2 was found to be concentration-dependent (Figure 6). The apparent K_m values of metformin transport by mouse Mate1-, mouse Oct1- and mouse Oct2-expressing cells were 0.3 ± 0.0, 1.8 ± 0.1 and 2.9 ± 0.4 mM, respectively. The V_{max}

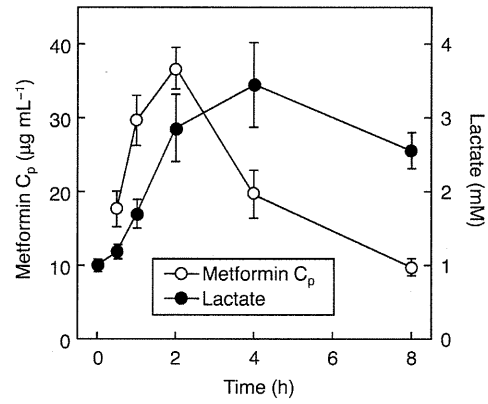

Figure 5

Lactate and metformin concentration–time profiles in *Mate1*$^{-/-}$ mice. Overnight-fasted mice were given 150 mg·kg^{-1} metformin (n = 8). Plasma concentration of metformin and blood lactate levels ere measured by HPLC and Lactate Pro respectively. Data represent mean ± SEM.

values were 5.3 ± 0.7 nmol·mg^{-1} protein·min^{-1}, 11.5 ± 2.3 nmol·mg^{-1} protein·2 min^{-1} and 18.5 ± 2.0 nmol·mg^{-1} protein·2 min^{-1} respectively.

Discussion

Genetic variants of drug transporters affect the pharmacokinetics of substrates and are involved in serious clinical outcomes. The organic anion transporting polypeptide 1B1 *(OATP1B1/SLCO1B1)* variant has been shown to increase plasma concentrations of simvastatin acid and is associated with statin-induced myopathy (Pasanen *et al.*, 2006; Link *et al.*, 2008). Our recent report suggested that the breast cancer resistant protein *(BCRP/ABCG2)* 421C>A variant causes the plasma concentration of sunitinib to increase and is associated with severe adverse effects to this drug such as skin reactions in the hands and feet (Mizuno *et al.*, 2010). In the case of metformin, a recent report demonstrated that MATE is involved in the excretion of metformin in humans by using the MATE inhibitor pyrimethamine (Kusuhara *et al.*, 2011). In addition, it was previously reported that the administration of metformin in the presence of pyrimethamine resulted in plasma concentrations of metformin 50 times higher than the therapeutic concentrations and also led to an increased blood lactate level (Ito *et al.*, 2010). In the present study, we focused on the clinical risk of metformin-induced lactic acidosis and carried out two experiments to examine the influence of *MATE* dysfunction on metformin-induced lactic acidosis in mice. On the continuous administration of metformin in drinking water, the mean plasma concentration of metformin in *Mate1*$^{+/+}$ mice was 1.4 μg·mL^{-1}, which is consistent with the clinical plasma concentration (Scheen, 1996; Toyama *et al.*, 2010). In *Mate1*$^{-/-}$ mice, the blood lactate level was significantly increased despite a lower dosage of metformin than in the *Mate1*$^{+/+}$ mice (Figure 1). After the same dose of metformin,

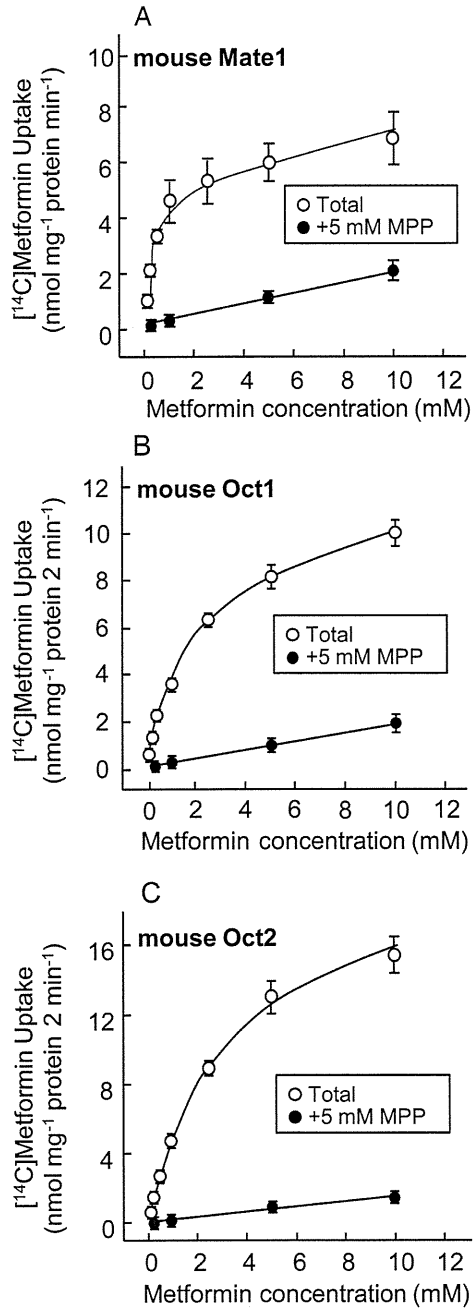

Figure 6

Concentration dependence of [^{14}C]-metformin uptake by mouse Mate1-, mouse Oct1- or mouse Oct2-expressing cells. The cells were incubated with [^{14}C]-metformin in the presence or absence of 5 mM MPP at 37°C for 1 min in mouse Mate1-expressing cells (A) and for 2 min in mouse Oct1- (B) or mouse Oct2-expressing cells (C). Data represent mean ± SEM.

administered as a bolus p.o., in *Mate1*$^{+/+}$ and *Mate1*$^{-/-}$ mice, severe lactic acidosis was observed in *Mate1*$^{-/-}$ mice, as shown by the levels of lactate, pH, HCO_3^- and several electrolytes, but not in the *Mate1*$^{+/+}$ mice (Figure 3 and Table 2). In addition, two of the *Mate1*$^{-/-}$ mice died after this acute metformin treatment, and the plasma creatinine concentration was also elevated in these metformin-treated *Mate1*$^{-/-}$ mice (Tables 1 and 2). These phenomena were reported in the patients with metformin-induced lactic acidosis (Misbin *et al.*, 1998; Tymms and Leatherdale, 1988; al-Jebawi *et al.*, 1998; Stades *et al.*, 2004). It was shown that the peak of blood lactate level followed the elevation of metformin concentration, and the high blood lactate level was maintained even though the metformin concentration was reduced immediately (Figure 5). These results suggest that metformin-induced lactic acidosis is caused by a completely dysfunctional MATE even when plasma concentration of metformin was within therapeutic range in *MATE*-reference carriers. Taken together, the data indicate that a dysfunctional *MATE* mutation could be a high risk factor for metformin-induced lactic acidosis.

In accord with our previous report on the pharmacokinetics of metformin, we found that in humans, the heterozygous *MATE* variant did not affect blood lactate levels (Figure 2) (Toyama *et al.*, 2010). In addition, the same results were obtained in *Mate1*$^{+/-}$ mice (Figure 1). This suggests that metformin-induced lactic acidosis is not just caused by the heterozygous *MATE* variant. On the other hand, there is no information about the blood lactate level in human homozygous *MATE* variant carriers due to low allelic frequencies of *MATE* variants with a loss of function (Chen *et al.*, 2009; Kajiwara *et al.*, 2009; Meyer zu Schwabedissen *et al.*, 2010). Metformin-induced lactic acidosis is also quite rare with 3 cases per 100 000 patient-years, but severe with a mortality up to 50% (Bailey and Turner, 1996; Misbin *et al.*, 1998). If possible, the nucleotide sequences of MATE should be determined in patients suffering from lactic acidosis after receiving metformin treatment.

The liver is a major pharmacological target organ for the action of metformin. In a previous report it was shown that the blood lactate level was elevated in *Oct1*$^{+/+}$ mice, but not in *Oct1*$^{-/-}$ mice, after metformin treatment (Wang *et al.*, 2003). Also hepatic concentrations of metformin were significantly lower in *Oct1*$^{-/-}$ mice than in *Oct1*$^{+/+}$ mice at similar plasma concentrations. Therefore, it was suggested that liver is the key organ responsible for metformin-induced lactic acidosis. In the present study we demonstrated that the hepatic concentration of metformin was 69-fold higher in *Mate1*$^{-/-}$ mice than in *Mate1*$^{+/+}$ mice, in spite of a 15-fold increase in the plasma concentration (Figure 4A and B). In *Mate1*$^{-/-}$ mice, the renal clearance of metformin was 18% of that in *Mate1*$^{+/+}$ mice, and the plasma concentration of metformin was higher (Tsuda *et al.*, 2009). In addition, it was reported that the MATE1 inhibitor pyrimethamine causes a 53 % reduction in hepatic clearance of metformin with respect to the liver concentration of metformin (Ito *et al.*, 2010). Taken together, these data indicate that a MATE1 dysfunction synergistically increased metformin accumulation in the liver due to the loss of urinary and biliary efflux of metformin, resulting in the development of lactic acidosis.

In addition to its effects in the liver, metformin, by activation of AMP-activated protein kinase (AMPK), also has a pharmacological effect in skeletal muscle (Zhou *et al.*, 2001). The AMPK activator AICAR has been reported to increase significantly the rate of lactate release within skeletal muscle

cells (Young *et al.*, 1996). A recent report showed that metformin was transported into skeletal muscle cells by OCT3 (Chen *et al.*, 2010). MATE1 is also expressed in skeletal muscle (Otsuka *et al.*, 2005) and in the present study it was found that the K_p value for metformin was increased in muscle from *Mate1*$^{-/-}$ mice (Figure 4G). Therefore, it is likely that MATE1 is responsible for metformin efflux from the skeletal muscle as well as in the kidney and liver.

Species differences exist in the MATE family (Yonezawa and Inui, 2011). The tissue distribution of the MATE family is reported to differ between humans and mice. MATE1 and MATE2-K are expressed in human kidney, whereas MATE2-K is not expressed in mice (Masuda *et al.*, 2006; Tsuda *et al.*, 2009). Therefore, *Mate1* knockout mice could represent a model of both MATE1 and MATE2-K deficiency in humans, because of similar affinities in mice and humans (Figure 6) (Tanihara *et al.*, 2007). The renal clearance of metformin in *Mate1*$^{+/-}$ mice was comparable with that in *Mate1*$^{+/+}$ mice despite the reduction of MATE1 expression (Toyama *et al.*, 2010). Taken together with the similar transport characteristics of MATE1 and MATE2-K (Tanihara *et al.*, 2007), it is assumed that the renal excretion of metformin was not affected in either homozygous *MATE1* or homozygous *MATE2-K* variant carriers. In the pharmacological targets such as liver and skeletal muscle, MATE1 was found but not MATE2-K (Yonezawa and Inui, 2011). In *Mate1*$^{-/-}$ mice, the hepatic and skeletal muscular K_p values for metformin were higher than those in the wild-type mice (Figure 4C and G). Therefore, it is anticipated that only the homozygous *MATE1* variant causes the elevation in metformin concentrations in the liver and skeletal muscle, even though renal excretion is not changed. In fact, in a previous case report, metformin-induced lactic acidosis was found to occur within the therapeutic concentration of metformin (Tymms and Leatherdale, 1988; al-Jebawi *et al.*, 1998). MATE1 is expressed in several tissues that are associated with metformin action, but MATE2-K is expressed only in the kidney (Yonezawa and Inui, 2011). Therefore, only the homozygous *MATE1* variant would affect the pharmacodynamics of metformin without a reduction in renal clearance.

In the present study, a dysfunction in MATE1 caused lactic acidosis after metformin treatment, accompanied by a reduction in the renal clearance of metformin and increase in hepatic accumulation. These findings indicate that MATE1 plays an important role in the pharmacodynamics of metformin. In conclusion, the homozygous *MATE* variant is one of the risk factors for metformin-induced lactic acidosis. These observations may provide new insights into the causes of metformin-induced lactic acidosis.

Acknowledgements

The authors are grateful to all the medical staff of the Department of Diabetes and Clinical Nutrition, Graduate School of Medicine, Kyoto University, especially to Dr Chizumi Yamada, Dr Kazuyo Fujita, Dr Akio Obara, Dr Norio Harada, Dr Kazutaka Nagai and Dr Shiho Takahara for excellent help. This study was supported by a grant-in-aid for Scientific Research (KAKENHI) from the Ministry of Education, Science, Culture, and Sports of Japan, and in part by the Nakatomi Foundation.

Conflicts of interest

None.

References

Bailey CJ, Turner RC (1996). Metformin. N Engl J Med 334: 574–579.

Becker ML, Visser LE, van Schaik RH, Hofman A, Uitterlinden AG, Stricker BH (2009). Genetic variation in the multidrug and toxin extrusion 1 transporter protein influences the glucose-lowering effect of metformin in patients with diabetes: a preliminary study. Diabetes 58: 745–749.

Chen L, Pawlikowski B, Schlessinger A, More SS, Stryke D, Johns SJ *et al.* (2010). Role of organic cation transporter 3 (SLC22A3) and its missense variants in the pharmacologic action of metformin. Pharmacogenet Genomics 20: 687–699.

Chen Y, Teranishi K, Li S, Yee SW, Hesselson S, Stryke D *et al.* (2009). Genetic variants in multidrug and toxic compound extrusion-1, hMATE1, alter transport function. Pharmacogenomics J 9: 127–136.

Ito S, Kusuhara H, Kuroiwa Y, Wu C, Moriyama Y, Inoue K *et al.* (2010). Potent and specific inhibition of mMate1-mediated efflux of type I organic cations in the liver and kidney by pyrimethamine. J Pharmacol Exp Ther 333: 341–350.

al-Jebawi AF, Lassman MN, Abourizk NN (1998). Lactic acidosis with therapeutic metformin blood level in a low-risk diabetic patient. Diabetes Care 21: 1364–1365.

Kajiwara M, Terada T, Ogasawara K, Iwano J, Katsura T, Fukatsu A *et al.* (2009). Identification of multidrug and toxin extrusion (MATE1 and MATE2-K) variants with complete loss of transport activity. J Hum Genet 54: 40–46.

Kimura N, Masuda S, Tanihara Y, Ueo H, Okuda M, Katsura T *et al.* (2005). Metformin is a superior substrate for renal organic cation transporter OCT2 rather than hepatic OCT1. Drug Metab Pharmacokinet 20: 379–386.

Kusuhara H, Ito S, Kumagai Y, Jiang M, Shiroshita T, Moriyama Y *et al.* (2011). Effects of a MATE protein inhibitor, pyrimethamine, on the renal elimination of metformin at oral microdose and at therapeutic dose in healthy subjects. Clin Pharmacol Ther 89: 837–844.

Link E, Parish S, Armitage J, Bowman L, Heath S, Matsuda F *et al.* (2008). SLCO1B1 variants and statin-induced myopathy – a genomewide study. N Engl J Med 359: 789–799.

Masuda S, Terada T, Yonezawa A, Tanihara Y, Kishimoto K, Katsura T *et al.* (2006). Identification and functional characterization of a new human kidney-specific H^+/organic cation antiporter, kidney-specific multidrug and toxin extrusion 2. J Am Soc Nephrol 17: 2127–2135.

Meyer zu Schwabedissen HE, Verstuyft C, Kroemer HK, Becquemont L, Kim RB (2010). Human multidrug and toxin extrusion 1 (MATE1/SLC47A1) transporter: functional

characterization, interaction with OCT2 (SLC22A2), and single nucleotide polymorphisms. Am J Physiol Renal Physiol 298: F997–F1005.

Misbin RI, Green L, Stadel BV, Gueriguian JL, Gubbi A, Fleming GA (1998). Lactic acidosis in patients with diabetes treated with metformin. N Engl J Med 338: 265–266.

Mizuno T, Terada T, Kamba T, Fukudo M, Katsura T, Nakamura E *et al.* (2010). ABCG2 421C>A polymorphism and high exposure of sunitinib in a patient with renal cell carcinoma. Ann Oncol 21: 1382–1383.

Otsuka M, Matsumoto T, Morimoto R, Arioka S, Omote H, Moriyama Y (2005). A human transporter protein that mediates the final excretion step for toxic organic cations. Proc Natl Acad Sci U S A 102: 17923–17928.

Pasanen MK, Neuvonen M, Neuvonen PJ, Niemi M (2006). SLCO1B1 polymorphism markedly affects the pharmacokinetics of simvastatin acid. Pharmacogenet Genomics 16: 873–879.

Pearlman BL, Fenves AZ, Emmett M (1996). Metformin-associated lactic acidosis. Am J Med 101: 109–110.

Safadi R, Dranitzki-Elhalel M, Popovtzer M, Ben-Yehuda A (1996). Metformin-induced lactic acidosis associated with acute renal failure. Am J Nephrol 16: 520–522.

Scheen AJ (1996). Clinical pharmacokinetics of metformin. Clin Pharmacokinet 30: 359–371.

Stades AM, Heikens JT, Erkelens DW, Holleman F, Hoekstra JB (2004). Metformin and lactic acidosis: cause or coincidence? A review of case reports. J Intern Med 255: 179–187.

Tanihara Y, Masuda S, Sato T, Katsura T, Ogawa O, Inui K (2007). Substrate specificity of MATE1 and MATE2-K, human multidrug and toxin extrusions/H^+-organic cation antiporters. Biochem Pharmacol 74: 359–371.

Toyama K, Yonezawa A, Tsuda M, Masuda S, Yano I, Terada T *et al.* (2010). Heterozygous variants of multidrug and toxin extrusions (MATE1 and MATE2-K) have little influence on the disposition of metformin in diabetic patients. Pharmacogenet Genomics 20: 135–138.

Tsuda M, Terada T, Mizuno T, Katsura T, Shimakura J, Inui K (2009). Targeted disruption of the multidrug and toxin extrusion 1 (Mate1) gene in mice reduces renal secretion of metformin. Mol Pharmacol 75: 1280–1286.

Tymms DJ, Leatherdale BA (1988). Lactic acidosis due to metformin therapy in a low risk patient. Postgrad Med J 64: 230–231.

Wang DS, Kusuhara H, Kato Y, Jonker JW, Schinkel AH, Sugiyama Y (2003). Involvement of organic cation transporter 1 in the lactic acidosis caused by metformin. Mol Pharmacol 63: 844–848.

Yonezawa A, Inui K (2011). Importance of the multidrug and toxin extrusion MATE/SLC47A family to pharmacokinetics, pharmacodynamics/toxicodynamics and pharmacogenomics. Br J Pharmacol 164: 1817–1825.

Young ME, Radda GK, Leighton B (1996). Activation of glycogen phosphorylase and glycogenolysis in rat skeletal muscle by AICAR-an activator of AMP-activated protein kinase. FEBS Lett 382: 43–47.

Zhou G, Myers R, Li Y, Chen Y, Shen X, Fenyk-Melody J *et al.* (2001). Role of AMP-activated protein kinase in mechanism of metformin action. J Clin Invest 108: 1167–1174.

Human Molecular Genetics, 2012, Vol. 21, No. 4 *765–775*
doi:10.1093/hmg/ddr508
Advance Access published on November 7, 2011

Molecular and cellular characteristics of *ABCA3* mutations associated with diffuse parenchymal lung diseases in children

Florence Flamein[1], Laure Riffault[1], Céline Muselet-Charlier[1], Julie Pernelle[1], Delphine Feldmann[3], Laurence Jonard[3], Anne-Marie Durand-Schneider[1], Aurore Coulomb[4], Michèle Maurice[1], Lawrence M. Nogee[6], Nobuya Inagaki[7], Serge Amselem[2], Jean Christophe Dubus[8], Virginie Rigourd[9], François Brémont[10], Christophe Marguet[11], Jacques Brouard[12], Jacques de Blic[13], Annick Clement[1,5], Ralph Epaud[14,15] and Loïc Guillot[1,*]

[1]Inserm U938 and [2]Inserm U933, UPMC, Univ Paris 6, France, [3]Department of Biochemistry, [4]Department of Pathology and [5]Department of Pediatric Pulmonology, Reference Center for Rare Respiratory Diseases in Children, Armand Trousseau Hospital, AP-HP, Paris, France, [6]Division of Neonatology, Department of Pediatrics, Johns Hopkins University School of Medicine, Baltimore, MD, USA, [7]Department of Diabetes and Clinical Nutrition, Graduate School of Medicine, Kyoto University, Kyoto, Japan, [8]Department of Pediatrics, Timone University Hospital, Marseille, France, [9]Institut de Puériculture de Paris, Paris, France, [10]Department of Pediatric Pulmonology and Allergology, Centre Hospitalo-Universitaire (CHU), Toulouse, France, [11]Department of Pediatric Pulmonology and Allergology, CHU, Charles Nicolle, Rouen, France, [12]Department of Pediatrics, CHU de Caen, Caen, France, [13]Department of Pediatric Pulmonology-Allergology, Université Paris Descartes, Hôpital Necker Enfants Malades, AP-HP, Paris, France, [14]Inserm U955, Créteil, France and [15]Université Paris Est, Créteil, France

Received August 29, 2011; Revised and Accepted October 29, 2011

ABCA3 (ATP-binding cassette subfamily A, member 3) is expressed in the lamellar bodies of alveolar type II cells and is crucial to pulmonary surfactant storage and homeostasis. *ABCA3* gene mutations have been associated with neonatal respiratory distress (NRD) and pediatric interstitial lung disease (ILD). The objective of this study was to look for *ABCA3* gene mutations in patients with severe NRD and/or ILD. The 30 *ABCA3* coding exons were screened in 47 patients with severe NRD and/or ILD. *ABCA3* mutations were identified in 10 out of 47 patients, including 2 homozygous, 5 compound heterozygous and 3 heterozygous patients. SP-B and SP-C expression patterns varied across patients. Among patients with *ABCA3* mutations, five died shortly after birth and five developed ILD (including one without NRD). Functional studies of p.D253H and p.T1173R mutations revealed that p.D253H and p.T1173R induced abnormal lamellar bodies. Additionally, p.T1173R increased IL-8 secretion *in vitro*. In conclusion, we identified new *ABCA3* mutations in patients with life-threatening NRD and/or ILD. Two mutations associated with ILD acted via different pathophysiological mechanisms despite similar clinical phenotypes.

INTRODUCTION

Pulmonary surfactant, a complex mixture of lipids and specific proteins located at the air–liquid interface, lowers alveolar surface tension, thereby preventing alveolar collapse at the end of expiration. It is synthesized by alveolar type-II cells, stored in lamellar bodies and secreted by exocytosis. Phospholipids make up ~90% of pulmonary surfactant.

Recent studies indicate a role for several genes in diffuse lung diseases (1–3). Genes implicated to date include the

*To whom correspondence should be addressed at: INSERM U938, Bâtiment Kourilsky, 184 rue du Faubourg Saint Antoine, 75012 Paris, France. Tel: +33 149284682; Fax: +33 143401748; Email: loic.guillot@inserm.fr

© *The Author 2011. Published by Oxford University Press. All rights reserved.*
For Permissions, please email: journals.permissions@oup.com

Downloaded from http://hmg.oxfordjournals.org/ at Kyoto University on May 13, 2012

Table 1. Genetic analysis results in the 10 children harboring homozygous and compound heterozygous (shaded) or heterozygous *ABCA3* mutations

Patient	NRD	Clinical outcome	*ABCA3* mutation cDNA level	Protein level	*ABCA3* SNPs dbSNPs rs# cluster id	*ABCA3* variants Missense variants in conserved amino acid
1	Yes	ILD	c.[3518C>G] + [3518C>G]	p.[T1173R] + [T1173R]	rs149532, rs13332514	
2	Yes	ILD	c.[757G>C] + [757G>C]	p.[D253H] + [D253H]		
3	Yes	Death	c.[1385T>G] + [2890G>A]	p.[L462R] + [G964S]	rs149532	
4	Yes	Death	c.[4747C>T] + c.[384delC]	p.[R1583W] + p.[S128Rfs]	rs149532	c.[450G>A] (het)
5	No	Death	c.[629G>T] + [3079G>C]	p.[G210V] + [A1027P]	rs149532	
6	Yes	ILD	c.[622C>T] + [4561C>T]	p.[R208W] + [R1521W]	rs149532, rs323043	
7	Yes	Death	c.[604G>C] + [907C>G]	p.[G202R] + [L303V]	rs149532, rs323043 (het), rs13332514	
8	Yes	Death	c.[2888A>G] + [?]	p.[Y963C] + [?]	rs149532 (het), rs323043 (het)	
9	Yes	ILD	c.[2125C>T] + [?]	p.[R709W] + [?]	rs149532	
10	Yes	ILD	c.[2614A>G] + [?]	p.[S872G] + [?]	rs149532 (het), rs323043, rs13332514 (het)	

het, heterozygous; NRD, neonatal respiratory distress; ILD, interstitial lung disease.

surfactant protein (SP)-B and SP-C genes (*SFTPB*, MIM 178640; and *SFTPC*, MIM 178620) and the ATP-binding cassette subfamily A member 3 gene (*ABCA3*, MIM 601615). SP-B deficiency has long been known to cause lethal neonatal respiratory distress (NRD) (4). More recently, *SFTPC* mutations were reported in newborns and infants with severe alveolar-interstitial syndrome (3,5). ABCA3 is a 1704-amino acid protein expressed selectively—but not specifically—in the lung, where it is found in the limiting membrane of lamellar bodies (1,6,7). ABCA3 is encoded by an 80 kb gene mapped to 16p13.3 in humans and is thought to regulate lipid transport and organization during lamellar body formation (8,9).

ABCA3 gene mutations are transmitted by autosomal recessive inheritance. As with SP-B deficiency, ABCA3 deficiency should be suspected in full-term infants with severe NRD refractory to maximal conventional treatment (10,11). In addition, *ABCA3* gene mutations have been found in children and young adults with interstitial lung disease (ILD) (1,3,12). For instance, the heterozygous c.875A>T (p.Glu292Val, p.E292V) *ABCA3* mutation was identified in several older children and young adults with desquamative interstitial pneumonitis (1). The large size and marked allelic heterogeneity of the *ABCA3* gene create challenges in mutation identification.

The objectives of this study were to identify and characterize *ABCA3* variations in a large population of pediatric patients with NRD and/or ILD. We identified new *ABCA3* gene mutations and found that these mutations were not associated with a specific expression profile of SP-B and SP-C in bronchoalveolar lavage fluid (BALF). Functional analysis of two mutations associated with ILD showed different pathophysiological mechanisms, despite the similar clinical phenotype.

RESULTS

Study patients

Of the 47 children enrolled in the study (Supplementary Material, Supporting Information 1), 23 (49%) were male and 24 (51%) female. The patients were from Europe ($n = 27$), North Africa ($n = 12$), Reunion Island ($n = 6$), West Africa ($n = 1$) and Haiti ($n = 1$). Among them, 6 (13%) were born prematurely (<36 weeks) and 31 (66%) had NRD. ILD developed in 31 (66%) patients, and 21 (36%) patients had both NRD and ILD. Nine (19%) patients died of respiratory failure.

Genetic analysis

Of the 47 patients, 10 had *ABCA3* mutations. We identified 15 mutations, including 13 that had not been described previously. The two mutations p.G210V and p.R208W have been already identified (13,14). There were 14 missense mutations and 1 heterozygous nonsense mutation (p.Ser128ArgfsX23, designated hereafter as p.S128Rfs) (Table 1).

Analysis of genomic DNA from the parents and kindred showed that the compound heterozygous p.R1583W/p.S128Rfs (Fig. 1A) and p.R208W/p.R1521W (Fig. 1B) mutations were inherited, as well as the homozygous mutations p.T1173R (Fig. 1C) and p.D253H (Fig. 1D). For the other mutations, genomic DNA samples from family members were not available.

None of these newly identified *ABCA3* mutations has been previously described as polymorphisms (http://ncbi.nih.gov/SNP). In addition, none of the new variants was detected in the 46 alleles from our 23 controls. Alignment of the human and other mammalian amino acid sequences (by Multiple Sequence Comparison using Log-Expectation, MUSCLE analysis) indicated that almost all the *ABCA3* mutations occurred in highly conserved residues (not illustrated). They were located across the protein in the extracellular domains (ECD1 and ECD2), as well as in internal domains (NBD1 and NBD2) (Fig. 2). Finally, complete *ABCA3* sequencing disclosed previously described single-nucleotide polymorphisms (SNPs) (Table 1), as well as a missense variant affecting a conserved amino acid in the patient harboring the c.[4747C>T]+[384delC] mutation.

In the 37 patients without *ABCA3* mutations, four SNPs were identified in the coding region of *ABCA3*. These SNPs were in exons 7, 9, 14 and 26, respectively, and did not induce amino acid variations. A missense variant in the conserved amino acid c.1059C>T was identified in nine children. We found these variants neither in the public polymorphism database nor in our controls.

Downloaded from http://hmg.oxfordjournals.org/ at Kyoto University on May 13, 2012

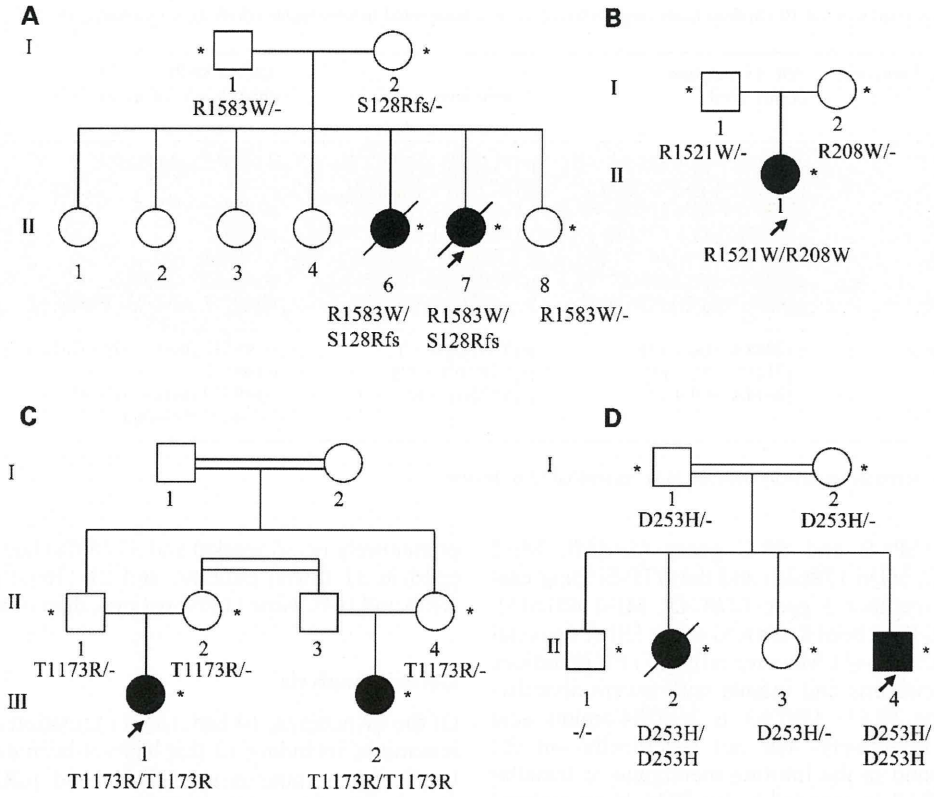

Figure 1. Pedigree of the families with the *ABCA3* mutations p.R1583W/p.S128Rfs (**A**), p.R1521W/R208W (**B**), p.T1173R/p.T1173R (**C**) and p.D253H/p.T1173R (**D**). Asterisks indicate family members with ABCA3 mutation analysis, and arrows indicate index patients.

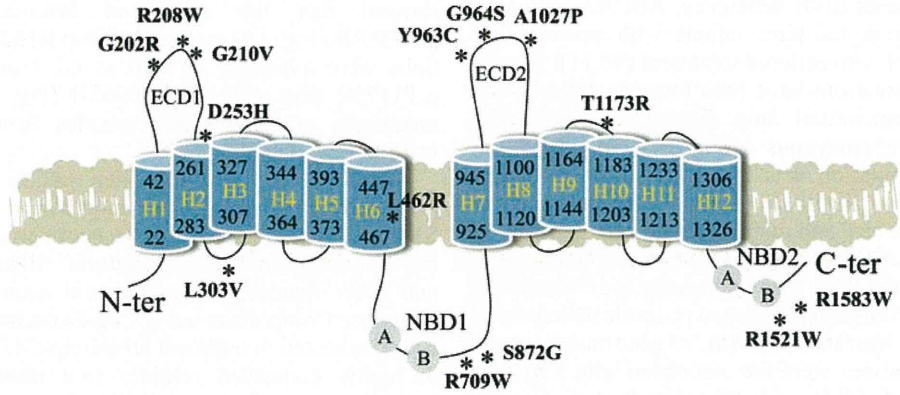

Figure 2. Schematic representation of the ABCA3 protein [N-terminal (N-ter) to C-terminal (C-ter) domains] and the location of the novel mutations (indicated by an asterisk). The 12 putative transmembrane helix (H1–H12) domains, two extracellular domains (ECD1 and ECD2) and two nucleotide-binding domains (NBD) (including the conserved motifs Walker A and B) are represented.

Characteristics of patients with *ABCA3* mutations

The characteristics of the 10 children with ABCA3 mutations are reported in Table 2. Among them, nine (90%) had NRD, five progressed to ILD and five died of respiratory failure (all during the first year of life).

Three children harboring homozygous and compound heterozygous mutations who developed ILD (patients 1, 2 and 6) were treated with methylprednisolone pulse for, respectively, 14 months (patient 1), 6 years (patient 2) and 11 years (patient 6, who is still on methylprednisolone pulse). They also received azithromycin for, respectively, 2 years (patient 1), 12 years (patient 2) and 2 years (patient 6), patients 2 and 6 still being treated. Two patients (patients 2 and 6) required prolonged oxygen supplementation for, respectively, 10 years (patient 2) and 11 years (patient 6, who is still on oxygen).

Two children harboring heterozygous mutations developed ILD (patients 10 and 9). The first child (patient 10) was

Downloaded from http://hmg.oxfordjournals.org/ at Kyoto University on May 13, 2012

Table 2. Clinical characteristics of the 10 patients with *ABCA3* mutations

	ABCA3-mutated patients ($n = 10$)
Sex: male/female, *n* (%)	4 (40)/6 (60)
Median age at onset in months (range)	0 (0–6)
Neonatal respiratory distress, *n* (%)	9 (90)
Hypoxemia, *n* (%)	10 (100)
Physical findings, *n* (%)	
Tachypnea	10 (100)
Retractions	10 (100)
HRCT findings, *n* (%)	
Ground-glass opacities	8 (100)
Lung cysts	3 (38)
Interlobular septal thickening	2 (25)
Consolidation	4 (50)
Lung biopsy, *n* (%)	
Type-II cell hyperplasia	6 (100)
Septal thickening	6 (100)
Mild fibrosis	5 (83)
Intra-alveolar macrophages	6 (100)
Outcome *n* (%)	
ILD/death	5 (50)/5 (50)

ILD, interstitial lung disease; *n* corresponds to the number of available patients' clinical data.

treated by monthly methylprednisolone pulse for 3 years and required oxygen supplementation for 8 months. The second one (patient 9) did not receive any treatment during the study period.

All 10 patients had clinical symptoms of respiratory failure. High-resolution computed tomography (HRCT) scans were available for eight patients and predominantly showed ground-glass opacities (Fig. 3A and Supplementary Material, Supporting Information 2). Lung biopsy was performed in six patients, all of whom had alveolar septal thickening, a few interstitial inflammatory cells (polymorphonuclear neutrophils and lymphocytes), uniform prominent type-II cell hyperplasia and accumulation of intra-alveolar macrophages (Fig. 3B). Electron microscopy was performed on a lung biopsy from the patient harboring the p.D253H mutation and showed abnormal lamellar bodies with dense inclusions (Fig. 3C).

BALF analysis

Western blot analysis of surfactant proteins (Fig. 4) was performed in seven patients, who had the following *ABCA3* mutations: p.D253H (patient 2), p.T1173R (patient 1), p.L462R/p.G964S (patient 3), p.G202R/p.L303V (patient 7), p.Y963C (patient 8), p.R1583W/p.S128Rfs (patient 4) and p.S872G (patient 10), respectively. SP-C (Fig. 4A) and SP-B (Fig. 4B) were detected at a size of 3.7 and 8 kDa in variable amounts, the smallest amount being found in the patient with the p.G202R/p.L303V *ABCA3* mutation (patient 7) in whom SP-C and SP-B are only faintly visible. This patient was the only one who cannot be weaned off mechanical ventilation before he died of respiratory failure. Interestingly, the two children harboring homozygous mutations (patients 1 and 2) have small but detectable amounts, which were nonetheless compatible with life. In contrast, patient 4, who died within the first month of life, had amount of SP-B and SP-C similar to control.

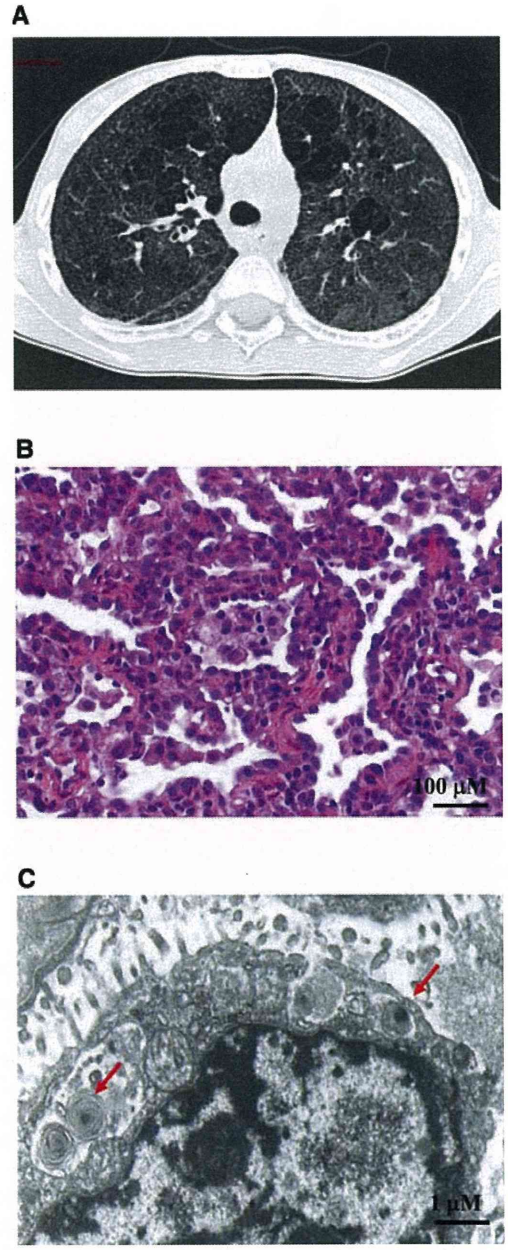

Figure 3. (**A**) HRCT scan, (**B**) hematoxylin and eosin (HE) staining of lung tissue and (**C**) electron microscopy of type-II cells from the patient (patient 2) harboring the *ABCA3* homozygous mutation p.D253H. Red arrows indicate lamellar bodies.

Characterization of ABCA3 mutations

The two mutations p.T1173R and p.D253H were deliberately chosen for subsequent functional studies because they were homozygous. Also, since past functional studies of ABCA3 focused mainly on NRD-associated mutations, it was crucial to study the consequences of these two mutations associated with progression towards ILD.

ABCA3 localization and processing. We first investigated the intracellular localization of the mutated ABCA3 protein.

Downloaded from http://hmg.oxfordjournals.org/ at Kyoto University on May 13, 2012

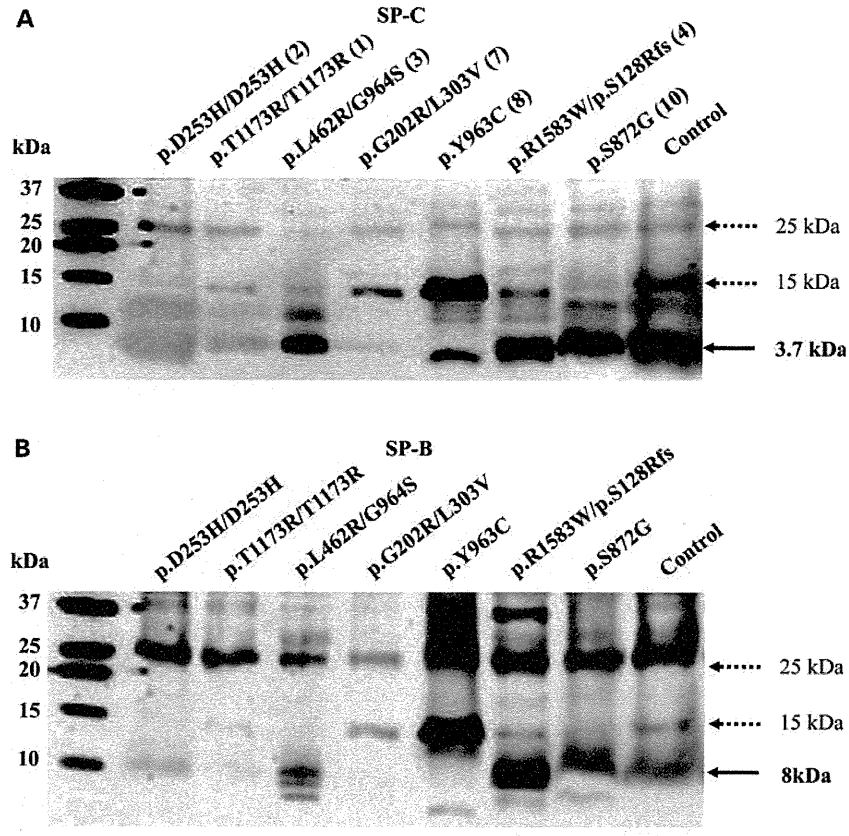

Figure 4. Western blot analysis of surfactant proteins B and C (SP-B and SP-C, respectively) in BALF from seven patients with *ABCA3* mutations and from a control without ILD. Dashed arrows indicate proSP-C (15 and 25 kDa) and proSP-B (15 and 25 kDa). Plain arrows indicate mature SP-C (3.7 kDa) and SP-B (8 kDa).

Similar to the WT protein, ABCA3 mutants co-localized with Lysotracker staining and partially with ERtracker staining (Fig. 5). ABCA3 might co-localize with ER during their folding. However, no accumulation in the ER was observed. The same results were obtained with transiently transfected cells (data not shown). Thus, p.D253H and p.T1173R mutants were not associated with a localization defect. ABCA3 expression was studied on protein extracts from A549-transfected cells. In WT, p.T1173R and p.D253H cells, anti-GFP antibody revealed two bands of 180 kDa (150 kDa ABCA3 + 30 kDa GFP) and 220 kDa (190 + 30 kDa GFP), respectively (Fig. 6). As previously suggested, these two bands might reflect two processing forms (15–18).

Lamellar bodies in ABCA3 WT, p.D253H and p.T1173R cells. Lamellar bodies were not observed in A549 cells (Fig. 7). As shown previously with HEK293 cells (15), transfection of ABCA3 in A549 cells is sufficient to induce lamellar body formation (Fig. 7). The p.D253H mutation induced abnormal lamellar bodies with electron-dense inclusions (Fig. 7, dashed arrows), consistent with the results of the patient's lung biopsy (Fig. 3C). In cells transfected with the p.T1173R mutation, abnormal lamellar bodies are the most frequently observed (irregularly arranged, phospholipid lamellae but eccentrically packed), even if some appeared almost normal.

Cytokine production by ABCA3 WT, p.D253H and p.T1173R cells. We next investigated whether ABCA3 mutants could induce inflammation. IL-8 was chosen as a well-known marker in inflammatory chronic lung disease. Using quantitative PCR (qPCR), we found that IL-8 mRNA levels were increased in p.T1173R cells (Fig. 8A). A significant, faint increase in IL-8 mRNA expression was also observed between WT and p.D253H cells. ABCA3 mRNA levels were similar in WT and mutated cells (data not shown), indicating that the increased IL-8 mRNA level in p.T1173R cells was not due to a transfection issue. At the protein level, ELISA results confirmed that A549 cells expressing the p.T1173R mutant produced more IL-8 than did WT cells (Fig. 8A). In contrast, IL-8 production by p.D253H cells was similar to that of WT cells (Fig. 8B). Finally, TGF-β and MCP-1secretions were similar between WT and transfected cells (data not shown).

IL-8 production is controlled chiefly by MAPK and NF-κB signaling (19). To determine whether these signaling pathways were involved in the observed IL-8 overproduction by p.T1173R cells, we used specific inhibitors. Treatment of cells with inhibitors of MAPK (p38, JNK, ERK1/2) and NF-κB showed that IL-8 production (in WT and mutant cells) was mainly ERK1/2 dependent. The lack of involvement of NF-κB was confirmed by measuring NF-κB promoter activity as done previously (20) (data not shown). However, with

Downloaded from http://hmg.oxfordjournals.org/ at Kyoto University on May 13, 2012

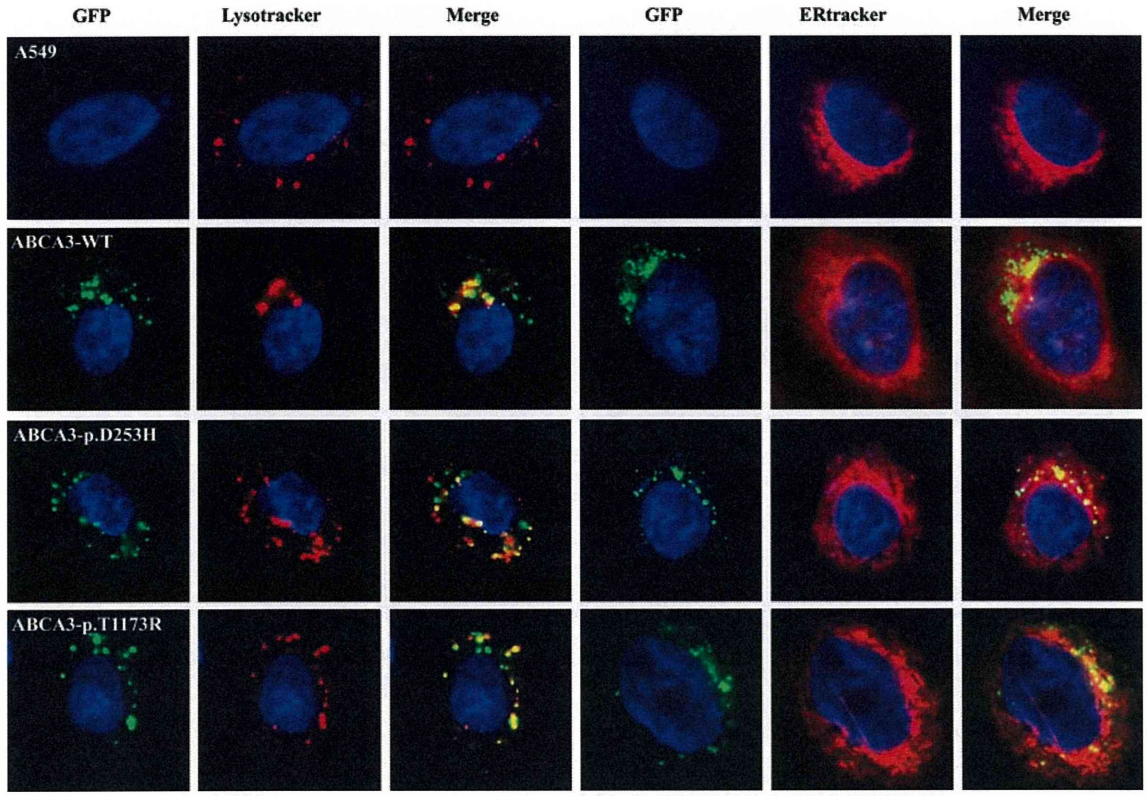

Figure 5. Intracellular localization of wild-type ABCA3 and of the p.D253H and p.T1173R mutants. A549 cells either non-transfected or transfected with mock vector, wild-type protein ABCA3-WT (**A**) or mutated proteins p.D253H (**B**) and p.T1173R (**C**) were analyzed using confocal microscopy. Lysotracker and ERtracker were used to stain lysosomes and the endoplasmic reticulum, respectively.

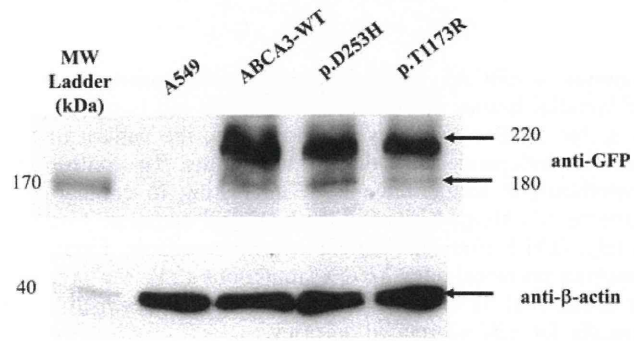

Figure 6. Western blot analysis of ABCA3 in cells transiently transfected with ABCA3-WT or the p.D253H or p.T1173R mutation. ABCA3 expression was detected using anti-GFP antibody (top panel). Equal loading was verified using anti-β actin antibody (bottom panel).

ERK1/2 inhibitor treatment, IL-8 production by p.T1173R cells remained increased compared with WT and p.D253H cells. These results suggest that, even if ERK1/2 signaling is involved in IL-8 production, another signaling pathway may be involved in the increased IL-8 production detected in p.T1173R cells.

Western blot and relative quantification of ERK1/2 phosphorylation confirmed that the observed IL-8 overproduction in p.T1173R cells was independent of ERK1/2 signaling. Finally, caspase 3/7 activity was similar in WT and mutant cells, indicating that these mutations did not induce apoptosis.

DISCUSSION

We identified 15 (13 novel) *ABCA3* mutations in 47 children (32%) who had NRD and/or ILD and no *SFTPB* or *SFTPC* mutations (5). None of these mutations was found in either the public polymorphism database or our controls. The amino acids affected by the mutations were conserved in mammalian *ABCA3* sequences. All 10 patients with *ABCA3* (21%) mutations had severe respiratory symptoms and abnormal chest imaging findings. Ninety percent of patients harboring *ABCA3* mutations had NRD. Finally, parents heterozygous for the p.R1583W, p.S128Rfs, p.R1521W or p.R208V mutations were not affected. In three patients, a mutation was found in a single allele but the clinical phenotype (NRD) may support the existence of a second mutation (in introns, deletions and so on) not detected by our sequencing method. Haploinsufficiency has been suggested as a mechanism leading to clinical phenotype emergence in patients with only one mutated allele (10,21). Similarly, $Abca3^{+/-}$ mice, despite normal respiratory function, had fewer lamellar bodies and altered surfactant lipid synthesis compared with wild-type mice, suggesting susceptibility to NRD or ILD (22). However, even if the observed clinical phenotypes are

Downloaded from http://hmg.oxfordjournals.org/ at Kyoto University on May 13, 2012

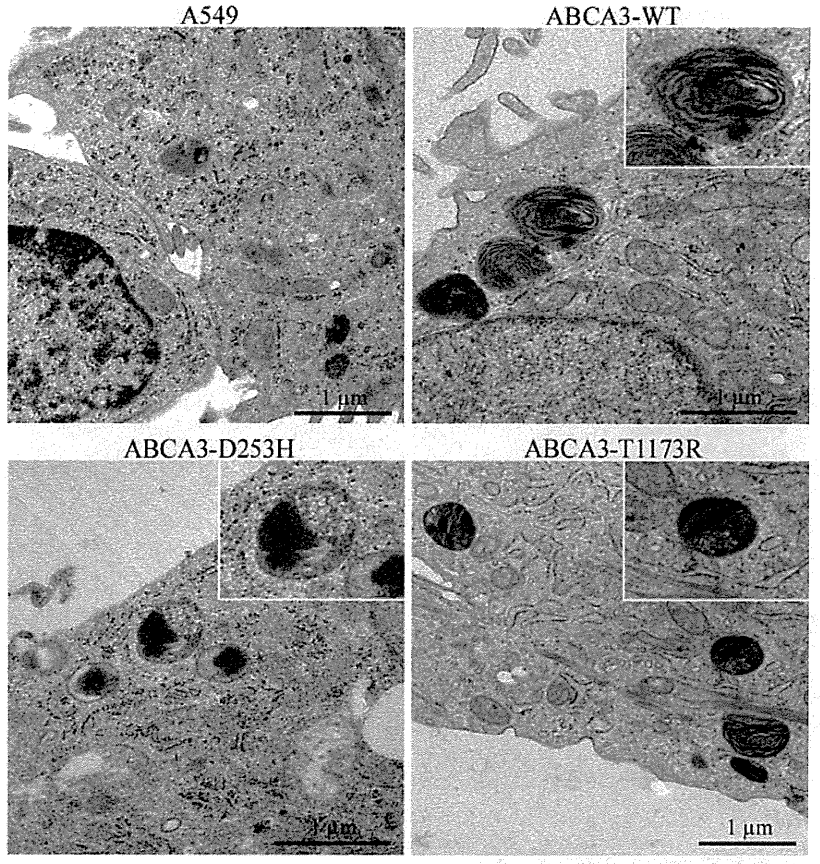

Figure 7. Lamellar body analysis. A549 cells transfected with mock vector (pEGFP-N1), ABCA3-WT (**A**), or mutated ABCA3-D253H (**B**) or ABCA3-T1173R-GFP were analyzed using electron microscopy.

compatible with *ABCA3* deficiency, we cannot conclude that *ABCA3* heterozygosis is responsible for this phenotype.

As previously described (1,11,13), some patients with *ABCA3* mutations had a less severe phenotype than that usually associated with *ABCA3* mutations (10). These variations in the clinical and radiological features may be related to the nature of the mutation (16). Previous studies showed that *ABCA3* mutations led to abnormal processing and/or trafficking of the ABCA3 protein (15), alterations in ABCA3 protein functions such as ATPase activity (16), or impaired lipid transport (23). Interactions with variants in other genes and/or with external factors such as viral infections may also influence the observed phenotype (24).

ABCA3 deficiency in full-term patients with NRD was shown previously to be associated with abnormal processing of SP-B and SP-C with an accumulation of precursors of SP-B and absence of mature SP-C (11). In our patients with *ABCA3* deficiency, we observed that SP-C and SP-B expression levels varied considerably across patients. Indeed, less severe patients had decreased amounts of SP-B and SP-C, whereas patient who died of respiratory failure showed normal expression of both proteins. This discrepancy may be explained by our technique of western blot, which is performed on lyophilized supernatant and improved the level of surfactant protein detection. It may also be explained by the function of ABCA3, which is critical for the proper formation of lamellar bodies and surfactant function but is not responsible for SP-B or SP-C synthesis. Hence, the pattern of SPs may be independent of the clinical status. To confirm the hypothesis, it would have been interesting to compare the patterns of siblings harboring the p.D253H mutation. Unfortunately, BALF from this patient was not available. Finally, as reported previously for *SFTPC* mutations (25), the presence or absence of SP-B and SP-C might be neither sensitive nor specific for *ABCA3*-related diseases.

Electron microscopy examination of a lung biopsy specimen is the reference standard for evaluating lamellar body characteristics and for providing a preliminary diagnosis prior to *ABCA3* gene analysis. Indeed, abnormal lamellar bodies with electron-dense inclusions have been described in association with *ABCA3* mutations in previous studies (10,21,26). However, electron microscopy cannot be performed routinely. The presence of abnormal lamellar bodies in the patient harboring the p.D253H mutation supports a pathogenic effect of this mutation. These abnormalities were also observed *in vitro* in p.D253H- and p.T1173R-transfected cells, suggesting that *ABCA3* abnormalities may consistently induce abnormal lamellar bodies. However, since we do not have the corresponding biopsy from the patient harboring the p.T1173R, we cannot draw a firm conclusion on this point.

Downloaded from http://hmg.oxfordjournals.org/ at Kyoto University on May 13, 2012

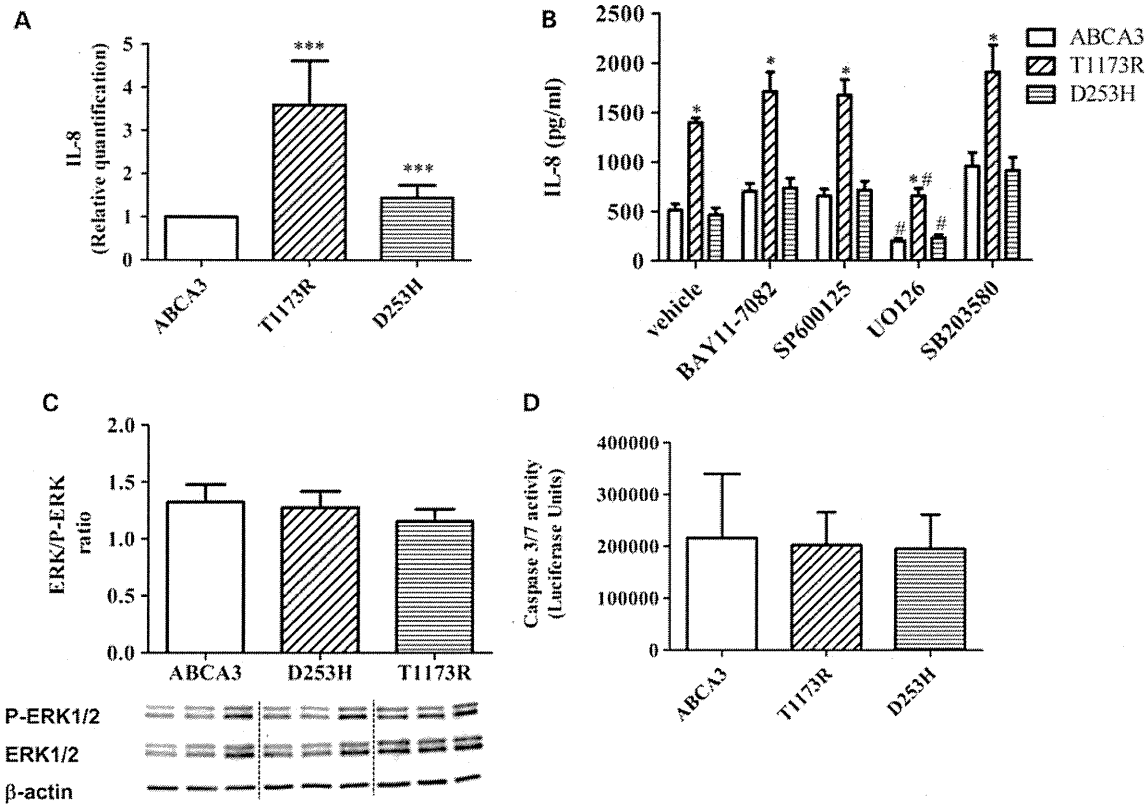

Figure 8. (**A**) IL-8 mRNA relative quantification was performed using qPCR. Results are representative of the mean ± SD of three experiments performed in triplicate. ***$P \leq 0.001$. (**B**) Role for MAPK and NF-κB-dependent signaling in IL-8 secretion by ABCA3-WT, D253H and T1173R cells. Cells were treated with 10 μM inhibitors of ERK1/2 (U0126), p38 (SB203580), JNK (SP600125) or NF-κB (BAY11-7082) for 24 h; *$P \leq 0.05$: ABCA3 versus T1173R; #$P \leq 0.05$: vehicle versus U0126. Supernatants were tested for IL-8 by ELISA. Data are means ± SD of three experiments performed in triplicate. (**C**) ERK1/2 phosphorylation measurement. Data are means ± SD of four experiments performed in triplicate. Results are expressed as P-ERK/ERK ratio (top panel). Western blot analysis of phospho-ERK1/2, total ERK1/2 and β-actin (bottom panel). (**D**) Caspase 3/7 activity. Data are means ± SD of three experiments performed in triplicate.

We performed *in vitro* experiments to elucidate the pathophysiological effects of two mutations associated with progression towards ILD, p.D253H and T1173R. These mutations did not alter the localization or maturation of the protein. Past functional studies on other *ABCA3* mutations showed localization/folding defects or functional defects (15,16,18,21,23,27). As pointed out recently, the effect of *ABCA3* mutations on lung epithelial cells depends on the ABCA3 protein defects (18). We found that the functional abnormalities differed between the two mutations. The p.D253H and p.T1173R mutations induced abnormal lamellar bodies. ABCA3 being a major transporter of phosphatidylcholine and phosphatidylglycerol into lamellar bodies, the lamellar body alterations suggest abnormalities in phospholipid trafficking that need to be characterized. The recent proteomic characterization of lamellar bodies may help to achieve this challenging objective (28). The p.T1173R mutation was also associated with increased production of IL-8, a well-known chemotactic molecule for neutrophils. Interestingly, increased IL-8 production was also detected in cells expressing *SFTPC* (Δexon 4 and the common p.I73T) mutations (29). In contrast, we do not find differences in TGF-β production, a cytokine that has been extensively studied in adults with idiopathic pulmonary fibrosis (30). Also, no differences in MCP-1 production were observed between WT and mutated cells. MCP-1 has been shown previously to contribute to the pathogenesis of pediatric ILD (31). However, in this study, none of the children had familial ILD, and surfactant genetic screening was not done, thus we do not know whether MCP-1 production is related to surfactant-associated disorders. In fact, surfactant genetic disorders are a subclass of pediatric ILD (2), which include various clinical phenotypes associated with specific clinical and biological features. Altered intercellular signaling was also shown recently in cells expressing *SFTPC* variants. CXCR1 and CCR2 expression by lymphocytes and neutrophils is probably dependent on an unidentified soluble mediator secreted by p.I73T cells (32). These studies, combined with our data, suggest that inflammatory pathways are involved in genetic surfactant disorders. However, better characterization of these pathways is required if specific treatments are to be sought.

In conclusion, although rare, ABCA3 deficiency should be considered in full-term newborns with severe respiratory distress and in older patients with ILD. Since *ABCA3* mutations lead to distinct functional defects, functional analysis of each *ABCA3* mutation is necessary to identify specific molecular targets that could be modulated or corrected by therapeutic agents.

Downloaded from http://hmg.oxfordjournals.org/ at Kyoto University on May 13, 2012